Supplementary Material

Statistics and Topology of Local Flame-Flame Interactions in Turbulent Flames

Ankit Tyagi[1], Isaac Boxx[2], Stephen Peluso[1], Jacqueline O'Connor[1]
[1]Mechanical and Nuclear Engineering, Pennsylvania State University, University Park, PA, USA
[2]German Aerospace Center (DLR), Stuttgart, Germany

A. Image Binarization Sensitivity

Most of the analysis in this paper relies on the adaptive threshold binarization of OH-PLIF images; here we have quantified the sensitivity of thresholding to image quality variations. The adaptive threshold binarization technique uses a threshold (C_T) based on Otsu's method in Matlab and the value of C_T changes from frame to frame. A distribution of C_T values from the time-series of binarized images can be used to calculate the standard deviation of C_T (σ_T) and this σ_T value can be used to obtain new thresholding values:

$$C_{T\_} = C_T - \sigma_T \quad \textbf{(1S)}$$

$$C_{T+} = C_T + \sigma_T \quad \textbf{(2S)}$$

Using these thresholding values, the flame-front edge can be traced and the total flame edge ($\mathcal{L}_f$) can be calculated. The normalized differences in the flame lengths from these new thresholds and the original thresholds can be reported as the sensitivity of the edge finding algorithm to the threshold value, $\mathcal{S}$:

$$\mathcal{S} = \left(\frac{\Delta\mathcal{L}_f}{\mathcal{L}_f}\right) \quad \textbf{(3S)}$$

Results from this sensitivity analysis they are shown in Figure 1S - Figure 12S for flames A-I. The plots on the left of these figures report the threshold values and their deviations for three fields of view; the plots on the right column report the sensitivity of the flame length calculation to threshold value. 100 frames, every fifth frame in each data set, are chosen to calculate the sensitivity. These results show that most of the images have little variability in flame length calculations to changes in thresholding values for binarization. For most cases, the $\mathcal{S}$ value is less than 10%, indicating that variations in the thresholding values do not change the identification of the flame-front locations significantly. With low values of $\mathcal{S}$, we are confident in the method's capabilities to capture the time-varying locations of the flame-front in these flames.

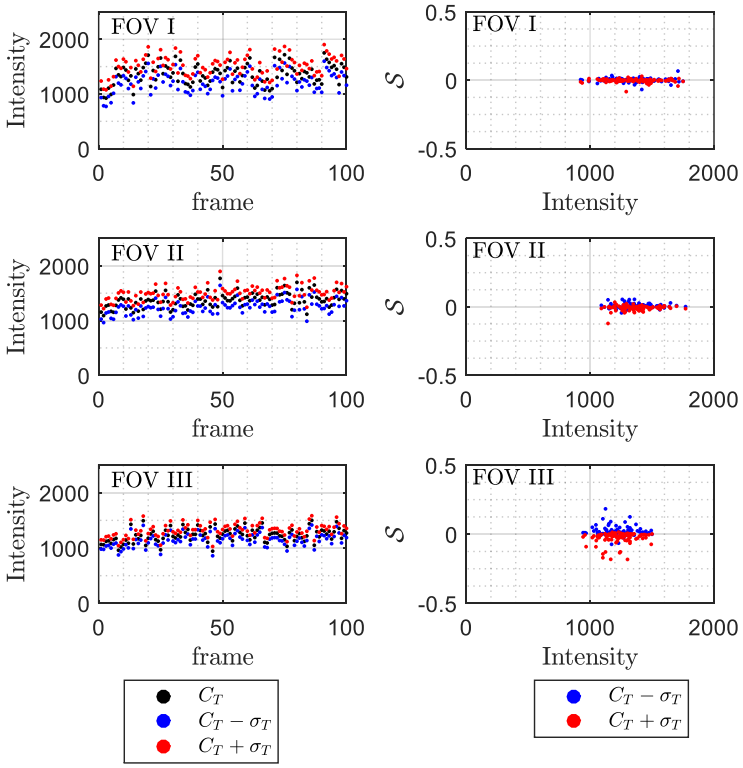

Figure 1S: A-single case binarization sensitivity

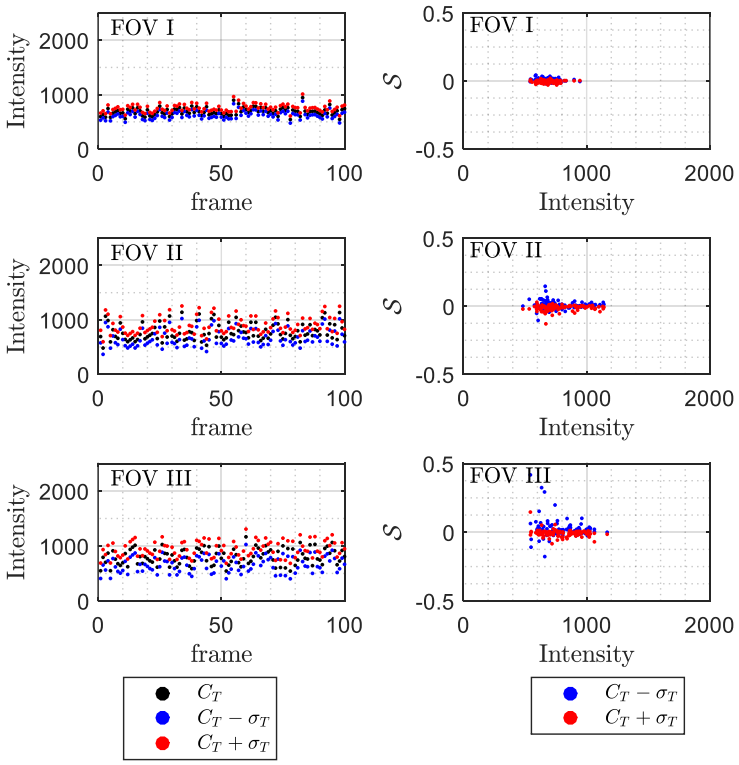

Figure 2S: C-single case binarization sensitivity

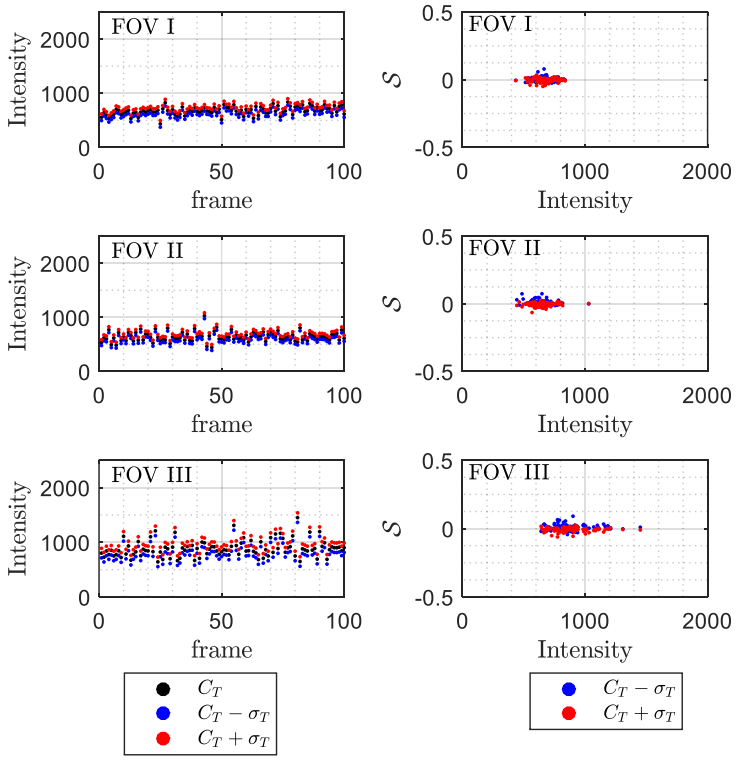

Figure 3S: E-single case binarization sensitivity

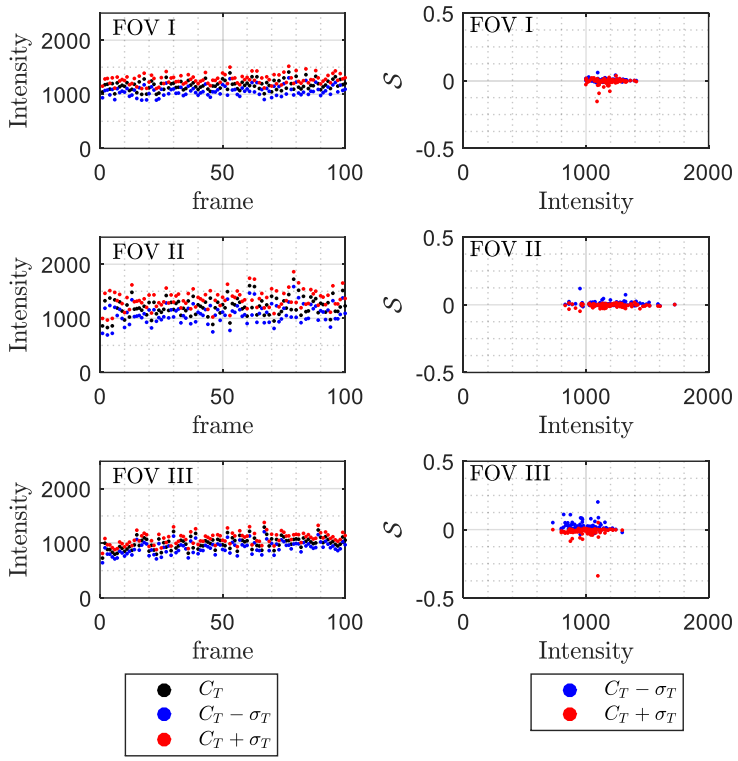

Figure 4S: A-dual case binarization sensitivity

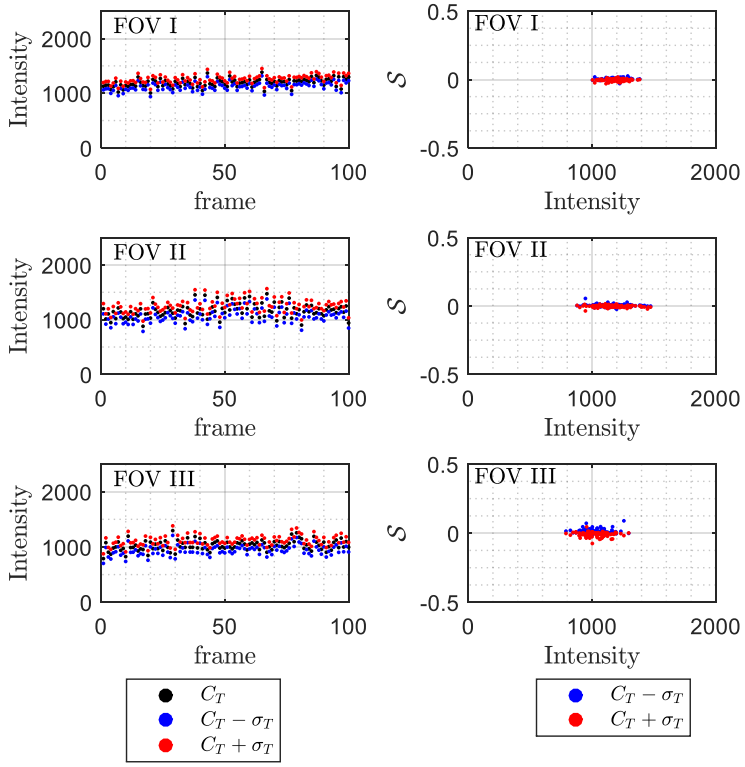

Figure 5S: B-dual case binarization sensitivity

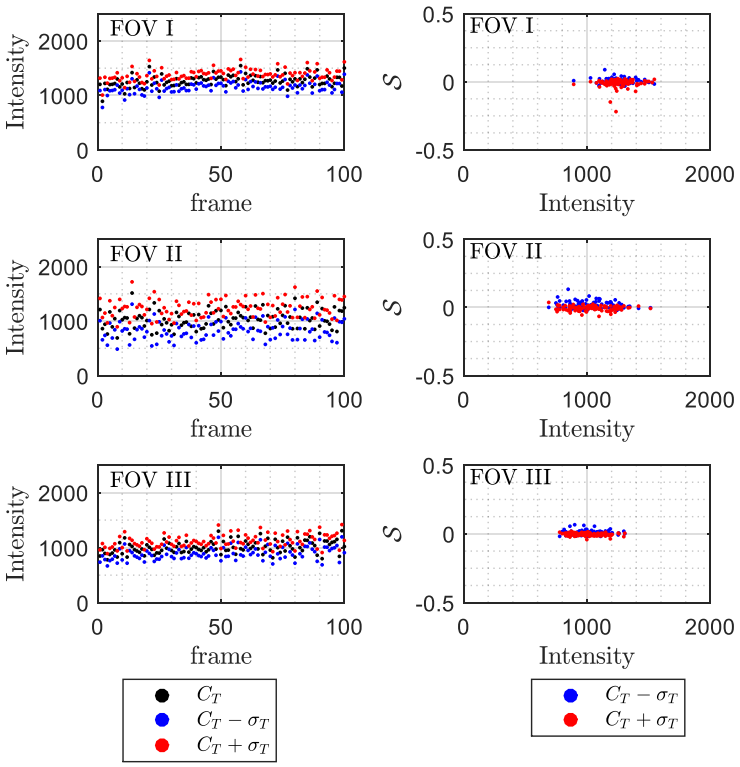

Figure 6S: C-dual case binarization sensitivity

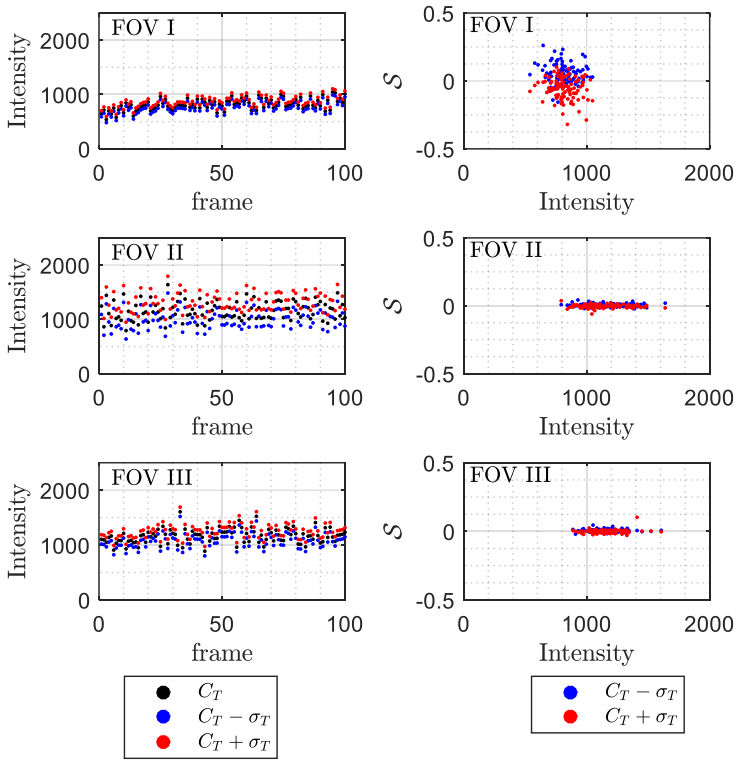

Figure 7S: D-dual case binarization sensitivity

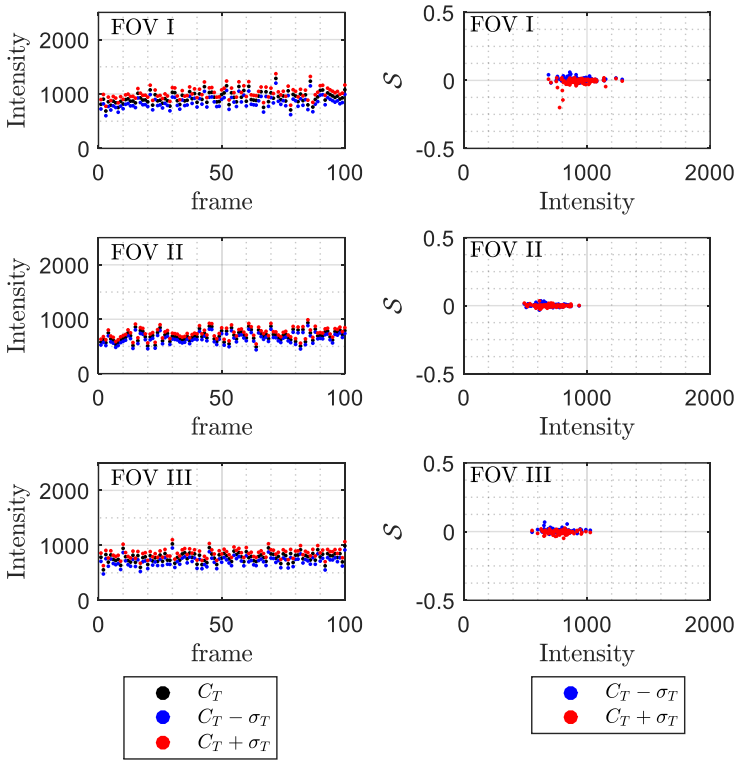

Figure 8S: E-dual case binarization sensitivity

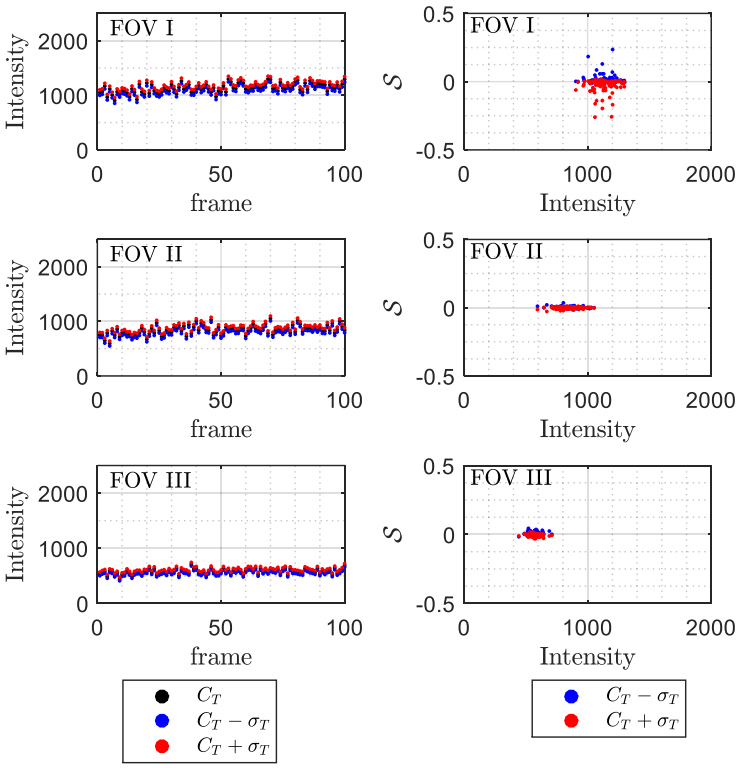

Figure 9S: F-dual case binarization sensitivity

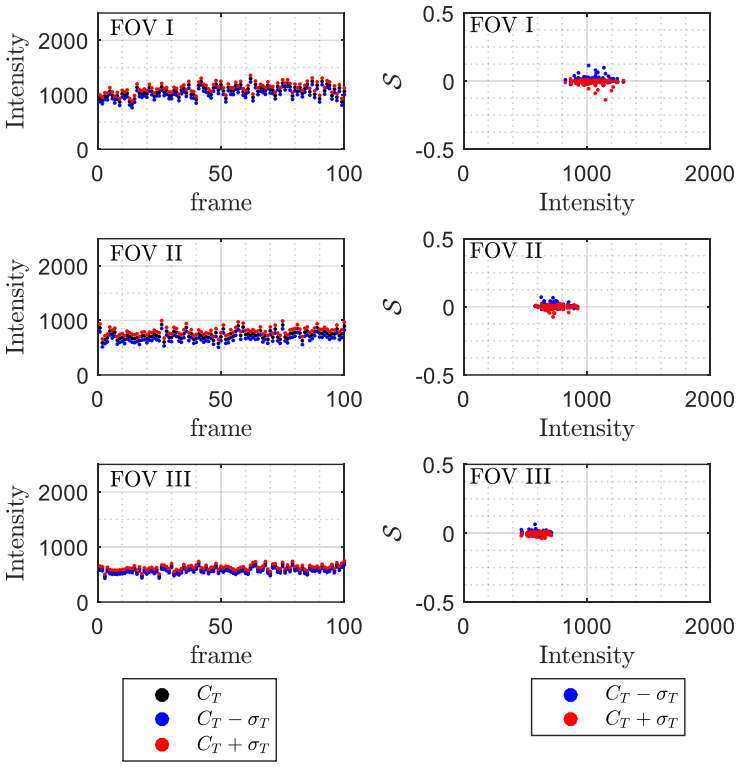

Figure 10S: G-dual case binarization sensitivity

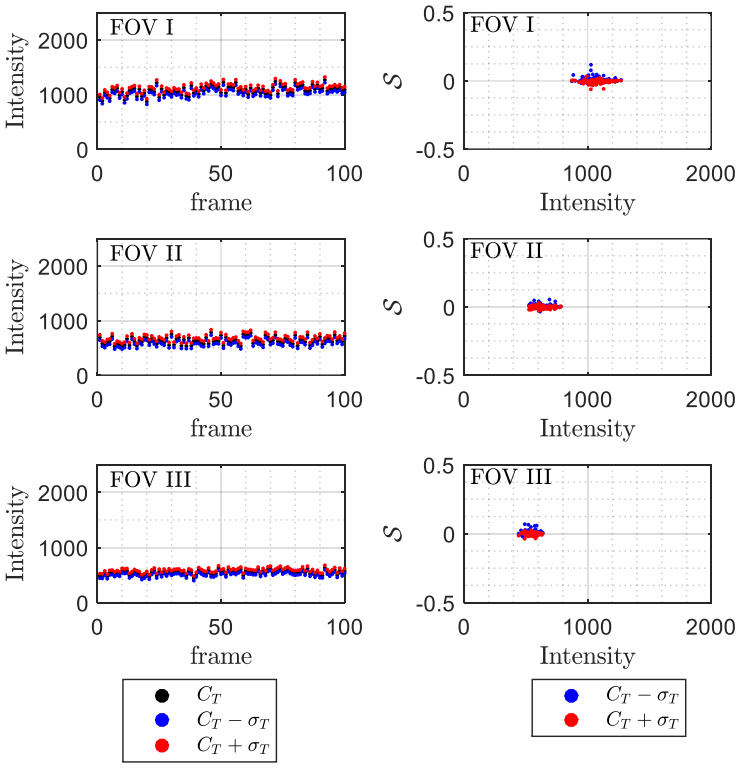

Figure 11S: H-dual case binarization sensitivity

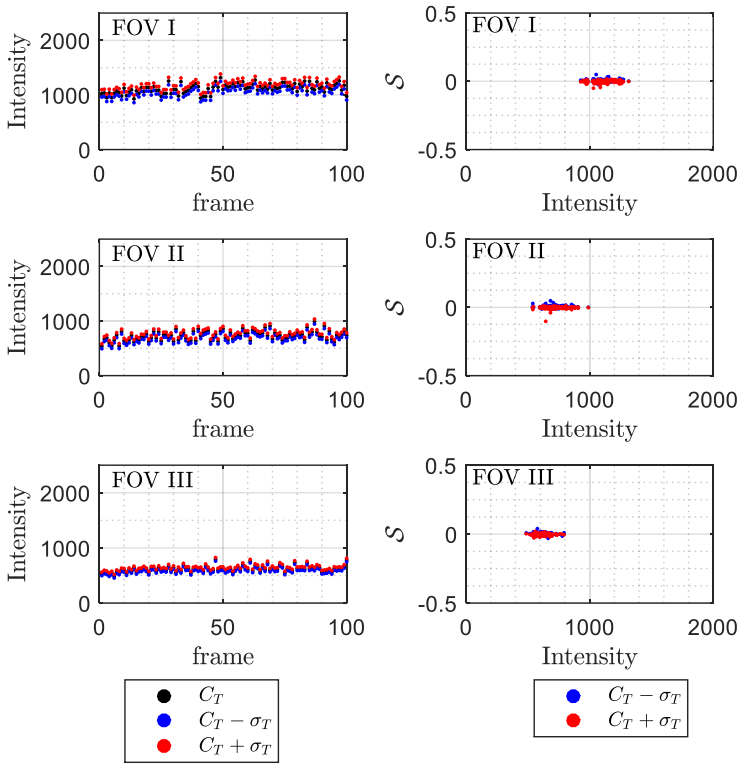

Figure 12S: I-dual case binarization sensitivity

B. Image Registration Methodology

Figure 13S illustrates the application of image registration on the OH-PLIF data for the current study. In this technique, operations are performed on binarized OH-PLIF images to estimate the displacement of flame edges between two consecutive images ('fixed' and 'moved'). Here, 'fixed' image refers to the image at any time of interest t_0 and 'moved' image refers to the consecutive image at time $t_0 + \Delta t$. The displacement field matches different features of flame edges between the two images and accounts for the local convection in the flowfield, as highlighted in Figure 13S(b). Translation operations are performed on the 'moved' image such that all common features of the 'fixed' and 'moved' images are matched (Figure 13S(c)) and resulting differences are recorded, which correspond to topological differences in these flames within Δt. An example of

such a difference is shown in Figure 13S(d). Figure 13S(e) and (f) show a time-sequence of unregistered and registered images for Case A.

In correctly utilizing this technique for identifying interactions in flames, an estimation of the displacement field for the 'moved' image is required. This estimation depends on the number of iterations and pyramid levels used in the algorithm. Here, the pyramid levels correspond to the levels of resolution (coarse-to-fine) utilized for alignment of flame edge features. For high turbulence flames, strong flame wrinkling occurs over a range of scales and the use of multi-resolution displacement field estimation is important for robust image alignment. Depending on the bulk flow velocities of the flames, the pyramid levels utilized for image registration vary from three to seven for cases in this study. These pyramid levels are selected by individually checking for convergence of the displacement fields for each case.

Distinguishing between reactant-side and product-side interactions from this technique requires appropriate processing of images obtained from image registration. Due to the closed shape of Bunsen flames, subtraction of a 'fixed' image from the registered 'moved' image results in topological differences with reactants being consumed in the middle. The length of flame edges from both 'fixed' (L_-) and registered 'moved' images (L_+) that trace the aforementioned topological differences are calculated and compared with each other. If L_- obtained from 'fixed' image is larger than L_+ obtained from the registered 'moved' image, the topological difference is registered as a reactant-side flame-flame interaction. Similarly, subtraction of the registered 'moved' image from the 'fixed' image yields with topological differences with product sides of the flame-fronts interacting. Additionally, corresponding flame edge lengths from 'fixed' and registered 'moved' images are calculated and compared, and topological differences

corresponding to larger 'fixed' image flame lengths ($L\_$) are registered as product-side flame-flame interactions

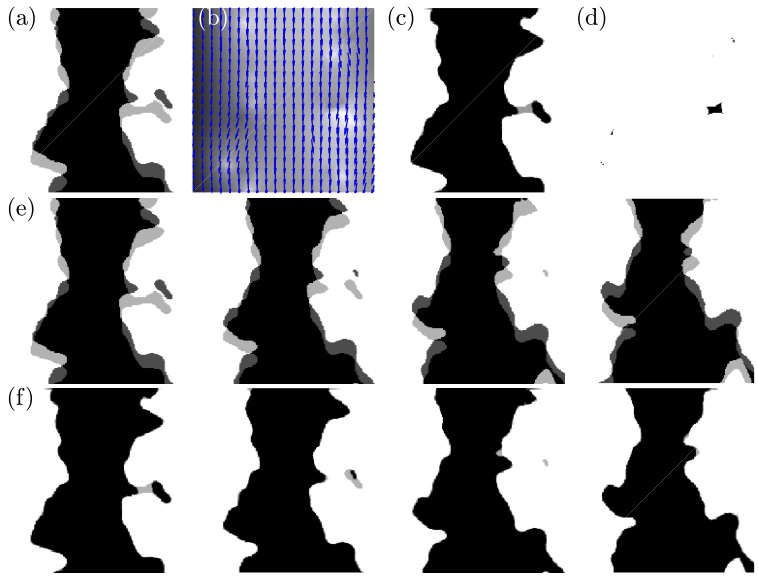

Figure 13S: Image registration methodology in identification of flame-flame interactions: (a) unregistered 'moved' image plotted on the 'fixed' image for two consecutive images, (b) vectors associated with displacement field for the 'moved' image plotted on the absolute displacement for each pixel in the image, (c) registered 'moved' image plotted on the 'fixed' image, and (d) differences between registered 'moved' and 'fixed' images. Time-series of (e) unregistered and (f) registered image pairs

C. Image Registration Sensitivity

Exact identification of the instant in time at which a flame-flame interaction event to occurs is limited by the sampling frequency of OH-PLIF system. For this study, the sampling time-step is 100 μs and interactions identified using the image registration algorithm occur within this time interval. The sensitivity of the image registration algorithm to the sampling rate can be studied by down-sampling the OH-PLIF data and comparing the areas of identified topological differences. A PDF plot of these areas for variation in time-steps ranging from 100-400 μs is shown in Figure 14S(a). This PDF shows that as the sampling time-step increases, fewer regions of small topological differences are identified. Similarly, more regions of larger topological differences are identified, as shown by the onset image in Figure 14S(a). Figure 14S(b) shows the variance of the

areas of these regions and the plot shows that the variance of these areas also increases as the time-step is increased.

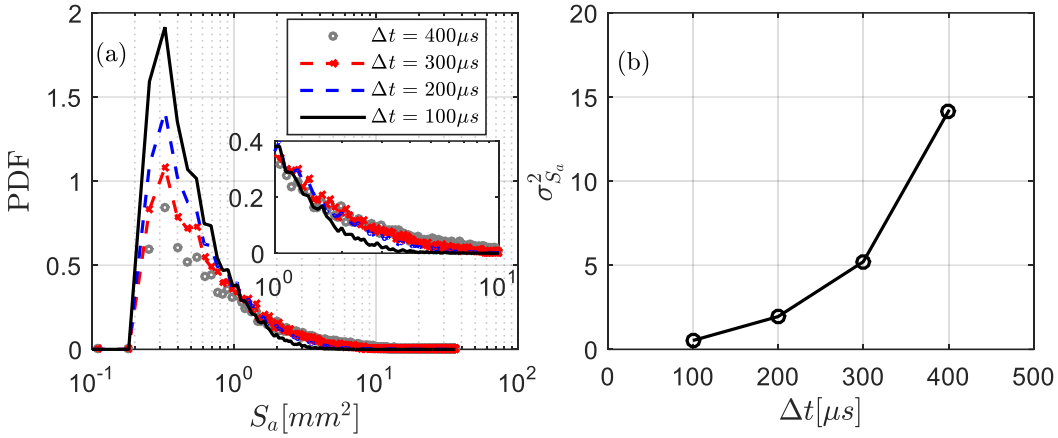

Figure 14S: Sensitivity of Δt on image registration methodology for single-flame case A in FOV I: (a) PDF plot of areas of topological differences identified through image registration for different sampling rates, and (b) plot of variance of the identified areas vs. the sampling time step (Δt)

The image registration timescale must be compared to two physical timescales that represent the flame behavior we are trying to capture: a consumption timescale and a convection timescale. The consumption timescale is estimated by approximating the time required for a flame-flame annihilation event to occur and represents the time scale associated with flame extinction using the flame speed at the extinction strain rate as the appropriate velocity-scale.

Time-scales associated with flame surface annihilations can be approximated using the concept of flame extinction velocity. For methane-air flames with inlet temperature of 300 K and pressure of 1 atm, the flame extinction velocity (u_{ext}) is approximately 2 m/s. From the PDF of areas in Figure 14S(a), the smallest observable region has an area of 0.25 mm^2 . Assuming a filamentarity of zero for this shape, the corresponding diameter is 0.56 mm and the perimeter is 1.76 mm. Using the extinction velocity, a time-scale associated with flame surface annihilation of this circular region is: τ_{ext} = 880 µs. Therefore, a sampling time-step of 100 µs for OH-PLIF measurements in this study is able to capture small-scale annihilation events.

The convective timescale is driven by the mean flow velocity, which varies from 12 m/s – 28 m/s in this study. Using 12 m/s and Δt = 100 μs as a baseline, we would expect the convective timescale at 28 m/s to be approximately half of that at 12 m/s. This is effectively the same as doubling the inter-frame time, where the sensitivity of the image registration method's ability to measure topological differences in that time is given by $\sigma_{S_a}^2$ = 1.95 mm^2, as shown by Figure 14S(b).

Figure 15S shows an example of the performance of image registration algorithm for various time-steps, which again can be interpreted as differences in inter-frame time, consumption times, and convective times. In each subplot, the difference between images at t_o and $t_o + \Delta t$ are shown and it is observed that as Δt increases, variation in the features of the flame surface increases within the times-step. As a result, incomprehensible topological changes with larges areas are registered.

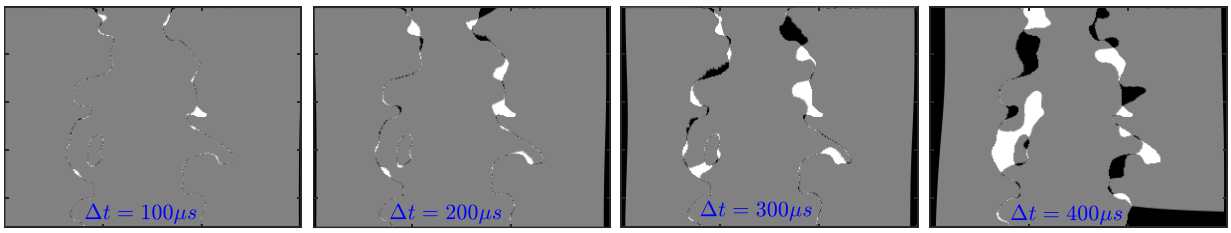

Figure 15S: Registered binarized images for various sampling time steps (Δt)

D. Uncertainty Analysis for Flame-Flame Interactions

Local interaction statistics presented in this study are quantified from two-dimensional imaging of three-dimensional turbulent flames; inferring three-dimensional flame topologies from planar measurements involves some uncertainties. In this analysis, we strive to differentiate an actual flame interaction event from a three-dimensional flame motion that may appear like an interaction

event in one plane. To understand the relative contribution from these two motions, we use the simultaneous s-PIV/OH-PLIF measurements to obtain the absolute instantaneous velocities at the centroid locations of interactions. In doing so, we assume that an interaction location with an out-of-plane velocity that is higher than the turbulent burning velocity is more likely to be a three-dimensional effect rather than a true interaction. While we recognize that a flame does not instantaneously propagate at the turbulent flame speed, it is a reasonable scaling for instantaneous, local flame speed in a turbulent flame. Equation (4S) is used to approximate the turbulent burning velocity for flames, where the laminar flame speed of the stoichiometric methane-air mixture is 0.4 m/s.

$$S_T = s_L \sqrt{1 + \left(\frac{u'}{s_L}\right)^2} \qquad \textbf{(4S)}$$

The turbulent burning velocities for these cases are shown in Table 1S, which are similar to u' fluctuations in the flowfield. Uncertainties in the instantaneous velocity are used to calculate a confidence interval $S_T \pm \delta S_T$. Uncertainty propagation of u' through Equation (4S) is performed and δS_T is calculated using the following equation:

$$\delta S_T = \left| \frac{u'}{\sqrt{u'^2 + s_L^2}} \right| \delta u' \qquad \textbf{(5S)}$$

Table 1S: Turbulent burning velocities

Case	S_T [m/s]	δS_T[m/s]	$S_T + \delta S_T$[m/s]
A-Dual	2.2	0.25	2.2 ± 0.25
C-Dual	3.6	0.34	3.6 ± 0.34
E-Dual	5.1	0.45	5.1 ± 0.45

Histograms of instantaneous out-of-plane (U_z) velocity components at the location of reactant-side interactions for dual-flames case A, C, and, E are shown in Figure 16S - Figure 18S. The percentage of interactions that are deemed "real" by this method is reported in each histogram, and ranges from 74-98%, with most cases being above 90%. The location of the turbulent burning velocities is marked with a green solid-line on the horizontal axis in each histogram, with uncertainties propagated through from the velocity measurement marked with black dashed-lines. The results shown here indicate that the image registration technique can potentially be a robust methodology to identify flame-flame interactions from high-speed OH-PLIF measurements, as the fraction of the detected interactions that meet our criteria is high.

Besides the out-of-plane motions resulting in uncertainties in identification of flame-flame interaction events, misalignment between the OH-PLIF laser sheet and the instantaneous flame surface can introduce uncertainties in this technique. Several studies have investigated this effect in turbulent premixed flames and how it impacts two-dimensional measurements[1][2][3][4]. In some of these studies, direct comparisons between three-dimensional flame surface curvatures and two-dimensional flame curvatures are performed for rectangular Bunsen flames and it is found that planar flame surface curvatures capture the characteristics of the three-dimensional flame surfaces very well. The study conducted by Bell and co-workers[4] also tabulates probabilities of flame structure shapes using 'shape factors' obtained from principal curvatures and it is reported that

[1] A.W. Skiba, On the Structure of Premixed Flames Subjected to Extreme Levels of Turbulence, University of Michigan, Ann Arbor (2017)
[2] L. Ma, Y. Wu, Q. Lei, W. Xu, C.D. Carter, 3D flame topography and curvature measurements at 5 kHz on a premixed turbulent Bunsen flame, Combustion and Flame 166 (2016) 66-75
[3] L. Ma, Q. Lei, T. Capil, S.D. Hammack, C.D. Carter, Direct comparison of two-dimensional and three-dimensional laser-induced fluorescence measurements on highly turbulent flames, Optics letters 42(2) (2017) 267-270
[4] J.B. Bell, M.S. Day, J.F. Grcar, M.J. Lijewski, J.F. Driscoll, S.A. Filatyev, Numerical simulation of a laboratory-scale turbulent slot flame. Proceedings of the combustion institute, 31(1) (2007) pp.1299-1307

high probabilities of shape factors of zero exist for rectangular Bunsen flames, indicating that for a large portion of the flame surface elements are nearly flat in one direction. While these results seem promising, three-dimensional effects cannot be ignored completely and future efforts will include assessing the uncertainties from this effect in carrying out the analysis in this study.

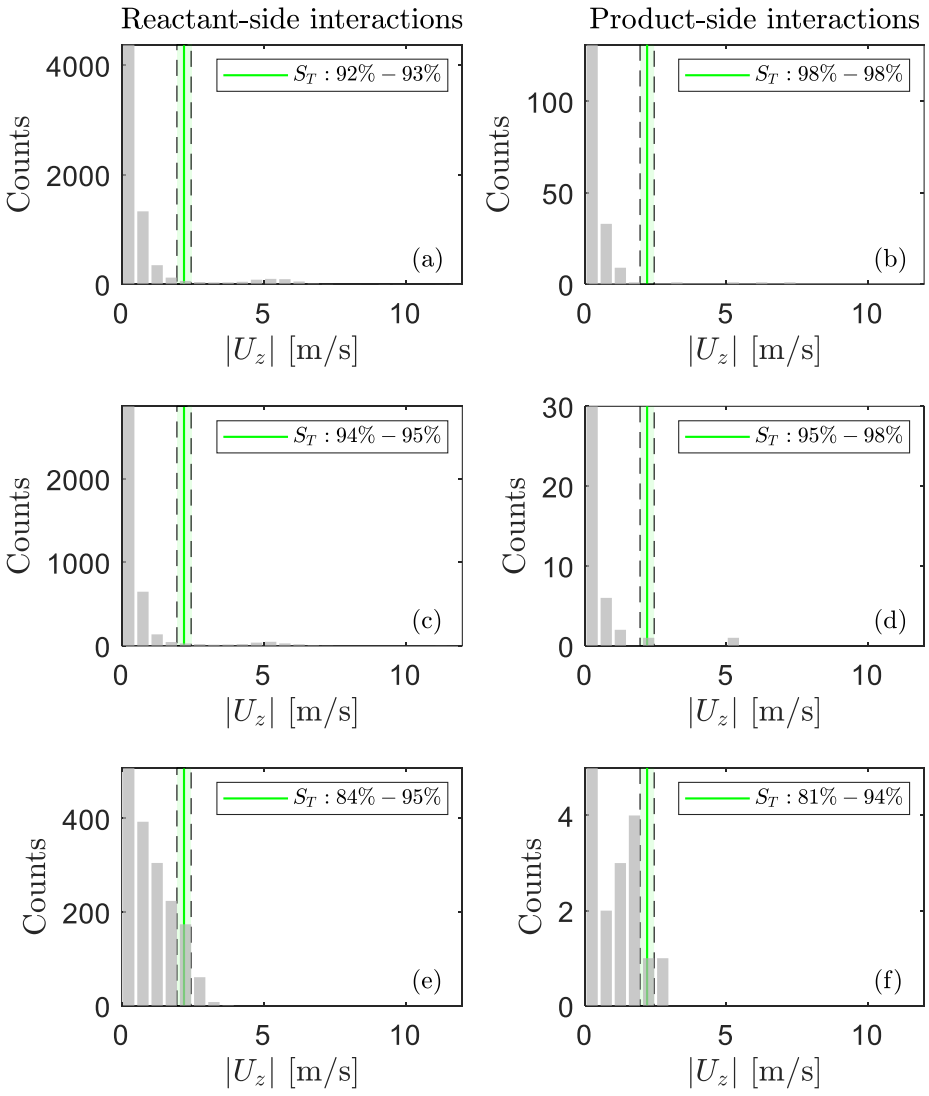

Figure 16S: Histograms of the magnitudes of out-of-plane (U_z) components of instantaneous velocity at the centroid locations of interactions in dual-flames case A: reactant-side interactions in (a) FOV I, (c) FOV II, and (e) FOV III; product-side interactions in (b) FOV I, (d) FOV II, and (f) FOV III. Vertical dashed lines correspond to the uncertainties on estimation of S_T from uncertainties in flowfield measurements

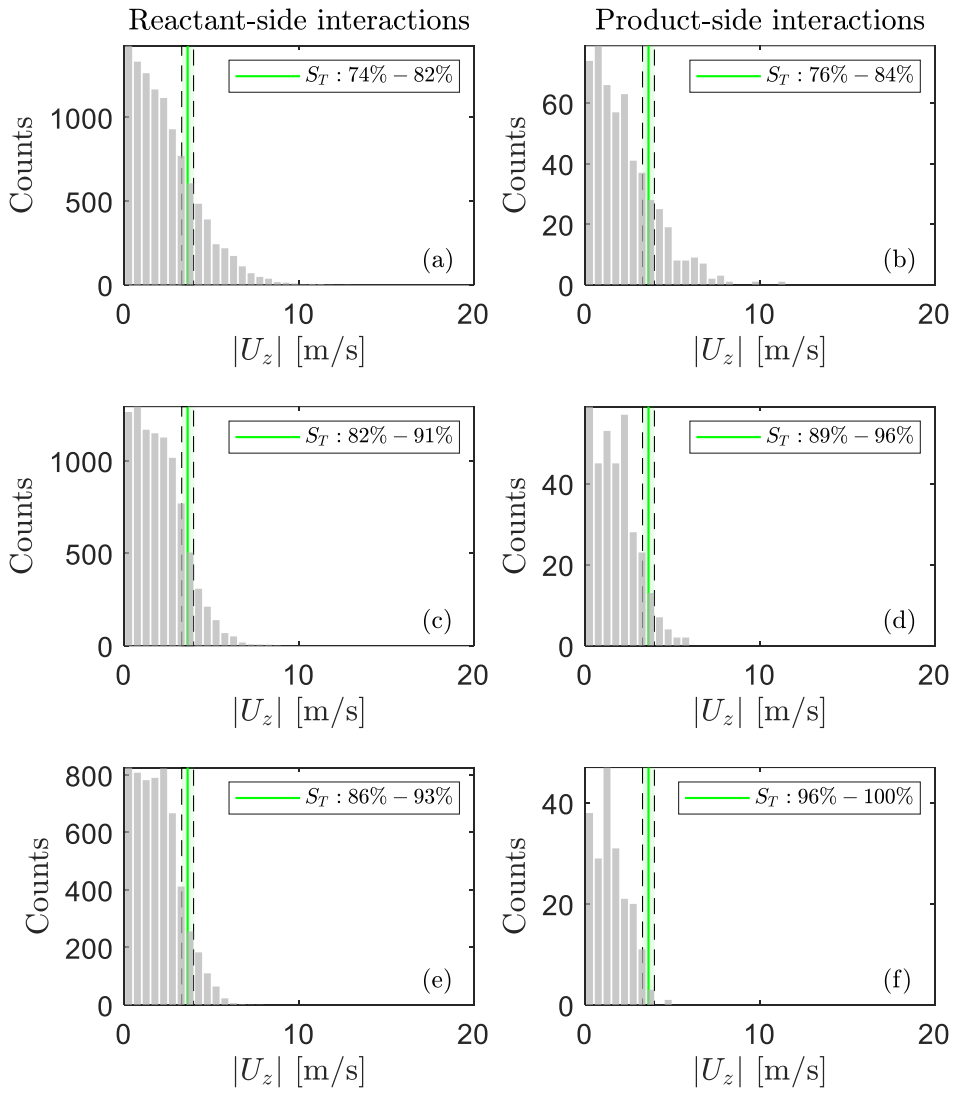

Figure 17S: Histograms of the magnitudes of out-of-plane (U_z) components of instantaneous velocity at the centroid locations of interactions in dual-flames case C: reactant-side interactions in (a) FOV I, (c) FOV II, and (e) FOV III; product-side interactions in (b) FOV I, (d) FOV II, and (f) FOV III. Vertical dashed lines correspond to the uncertainties on estimation of S_T from uncertainties in flowfield measurements

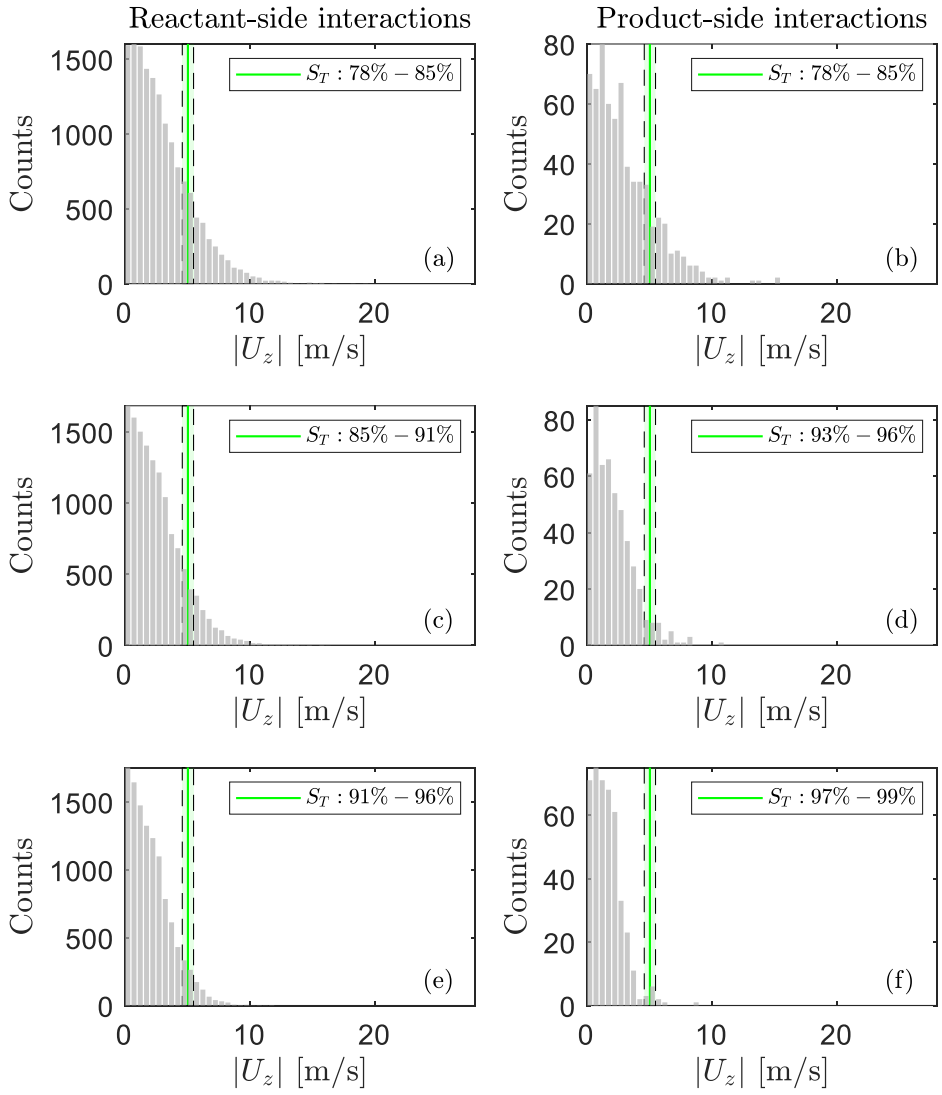

Figure 18S: Histograms of the magnitudes of out-of-plane (U_z) components of instantaneous velocity at the centroid locations of interactions in dual-flames case E: reactant-side interactions in (a) FOV I, (c) FOV II, and (e) FOV III; product-side interactions in (b) FOV I, (d) FOV II, and (f) FOV III. Vertical dashed lines correspond to the uncertainties on estimation of S_T from uncertainties in flowfield measurements

E. Conditioning of Turbulence Length-Scales

Previous studies have conditioned velocity fields and turbulent statistics on whether the vector is in the reactants or the products, as gas expansion across the flame affects local turbulence[5], [6]. In this study, we are interested in the turbulent length scales at a range of progress variables. Initially, length-scale results from conditioning velocity fields on reactants/products were compared with those from unconditioned velocity fields. For reactant-conditioned integral length-scales, length scales at progress variables of $\bar{c}$=0.0-0.4 produced physically-meaningful results because the vectors at these progress variables are statistically more likely to be in the reactants. Similarly, product-conditioned integral length-scales results were physically meaningful for locations of $\bar{c}$=0.7-0.9. Autocorrelation functions obtained for conditioned statistics outside these $\bar{c}$ ranges for both reactant and product conditioned cases followed the same general trends as the conditioned cases but are noisy and cannot be utilized for length-scale calculations. Hence, unconditioned autocorrelations are utilized for calculations of integral length scales in *x* and *y* directions in this study.

Figure 19S and Figure 20S show the development of unconditioned, reactant-conditioned, and product-conditioned integral length-scales (L_{11} and L_{22}) and velocity-scales (u_x', u_y' and u_z') at various downstream locations of $\bar{c}$ for FOV I of dual-flames case E.

[5] S. Pfadler, M. Löffler, F. Dinkelacker, A. Leipertz, Measurement of the conditioned turbulence and temperature field of a premixed Bunsen burner by planar laser Rayleigh scattering and stereo particle image velocimetry, Experiments in fluids 39 (2005) 375-384

[6] T.M. Wabel, A.W. Skiba, J.F. Driscoll, Evolution of turbulence through a broadened preheat zone in a premixed piloted Bunsen flame from conditionally-averaged velocity measurements, Combustion and Flame 188 (2018) 13-27

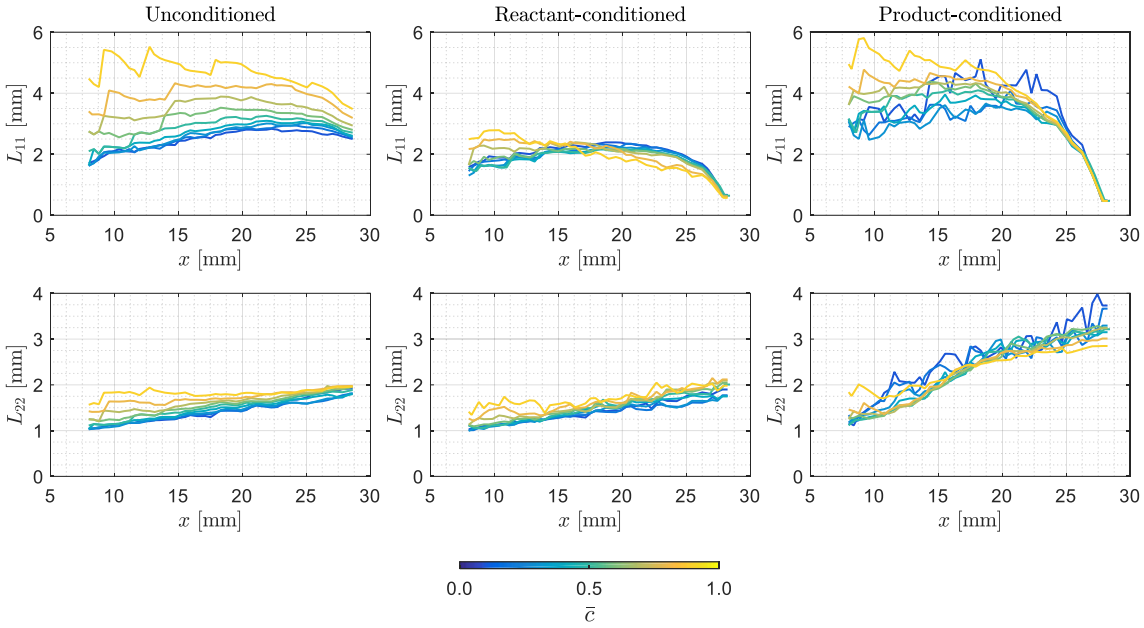

Figure 19S: Plots of L_{11} and L_{22} as a function of downstream distance for various $\bar{c}$ locations. Columns correspond to unconditioned, reactant-conditioned, and product-conditioned length-scales.

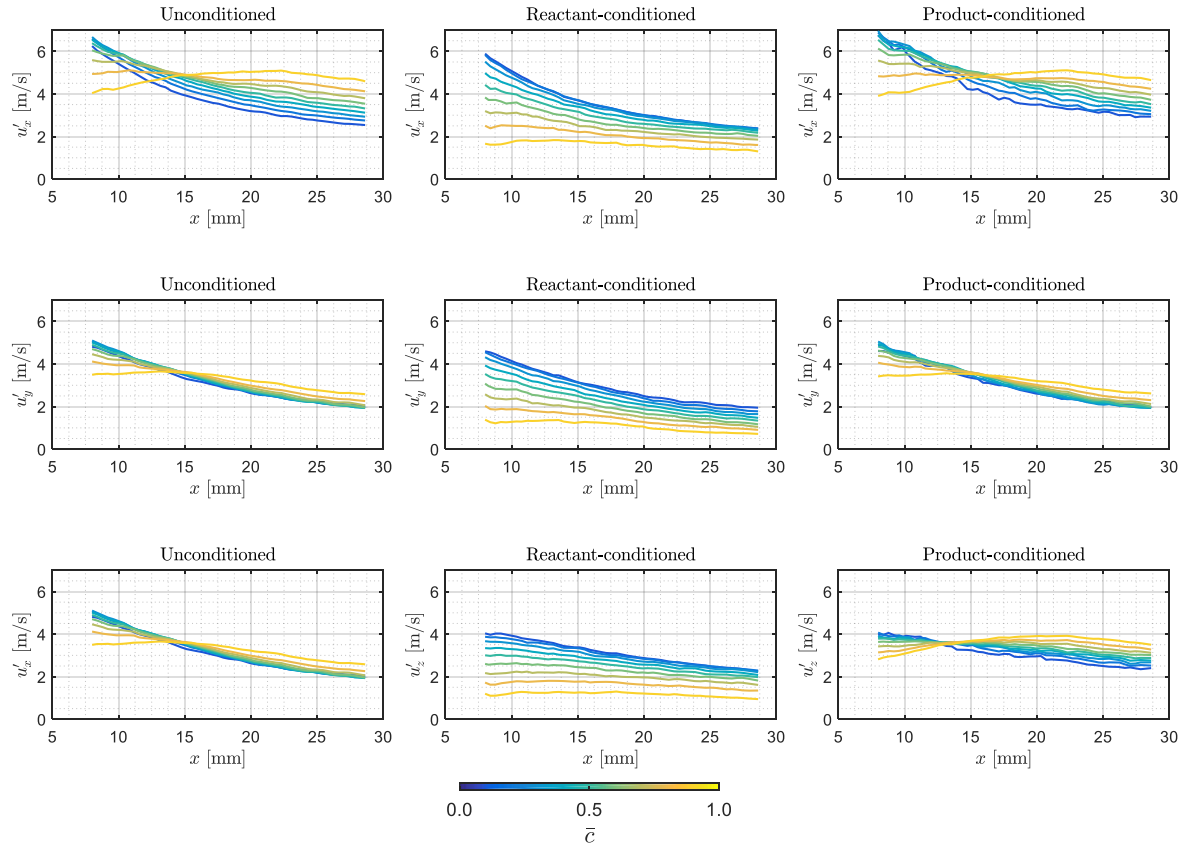

Figure 20S: Plots of u_x', u_y', and u_z' as a function of downstream distance for various $\bar{c}$ locations. Columns correspond to unconditioned, reactant-conditioned, and product-conditioned velocity-scales.